A 3D image analysis of intermetallic inclusions

Estelle Parra-Denis, Christophe Ducottet, Dominique Jeulin

A 3D image analysis of intermetallic inclusions

Estelle Parra-Denis
Centre de Morphologie Mathématique
Mines ParisTech
35 rue Saint-Honoré, 77300 Fontainebleau, France

Christophe Ducottet
Université de Lyon
F-42023, Saint-Etienne, France
and
Laboratoire Hubert Curien
CNRS UMR5516
F-42000, Saint-Etienne, France
and
Université de Saint-Etienne
Jean Monnet, F-42000, Saint-Etienne, France

Dominique Jeulin
Centre de Morphologie Mathématique
Mines ParisTech
35 rue Saint-Honoré, 77300 Fontainebleau, France

Abstract: The problem of 3D shape characterisation has been intensively studied lately, because computing power is greatly increasing and image acquisition is more efficient, with new real 3D image acquisition methods like microtomography. The material studied in this work is a 5xxx aluminium alloy. It contains intermetallic particles which control both formability and surface aspect. During the industrial process used to transform slabs into plates, particles are broken and redistributed in the sheet space. In this paper, the shape of the intermetallic particles originating from the solidification process of aluminium alloys is studied. These particles are observed as being very complex. Modelling their shape requires a single approach based on 3D morphological analysis. A description of the shape of each intermetallic particle is given, using parameters and distribution measures. This paper also presents an original way to study the evolution of particles at different stages of deformation of the material and the evolution of its orientations.

Keywords: X-ray microtomography; 3D complex shape; segmentation; morphological analysis; 3D shape characterisation.

1 Introduction

The material studied in this paper is an aluminium alloy used in the automotive industry for inner panels. It contains intermetallic particles and voids, both formed during solidification. The industrial process used to transform aluminium slabs into plates is hot rolling. During this stage, the structure of the material undergoes an important evolution under the applied stress. One observes that particles are broken and randomly distributed, and the distributions of the size and shape of the particles and voids change (Baldacci, 2003).

An examination of the phenomenon was made with a Scanning Electron Microscope (SEM) (Feuerstein, 2006). The complex shape of each type of particle was highlighted, implying the use of a real three-dimensional method to observe the shapes.

The aim of this work was to measure particles and to compare different states of deformation during the hot rolling process (Parra-Denis *et al.*, 2005a–b).

The next part of this paper presents 3D images obtained by an X-ray microtomography (Buffiere *et al.*, 1999). The third part shows the method used to segment 3D images (Parra-Denis, 2005b). The fourth part focuses on the different morphological parameters that were selected (Klette and Zamperoni, 1996; Soille, 1999). The fifth part gives some preliminary results. Finally, a conclusion is given and available perspectives are presented.

2 3D images

The studied aluminium alloy is a 5xxx aluminium. It contains two types of intermetallic particles: iron-containing particles (Al_xFe) and silicon-containing particles (Mg_2Si). Both types of particles were formed during the solidification process and show three-dimensional complex shapes. Voids can be seen as the third type of object (as shown in Figure 1).

Figure 1 Example of image of aluminium alloy 5xxx obtained by X-ray microtomography (displayed with Aphelion© 3D software)

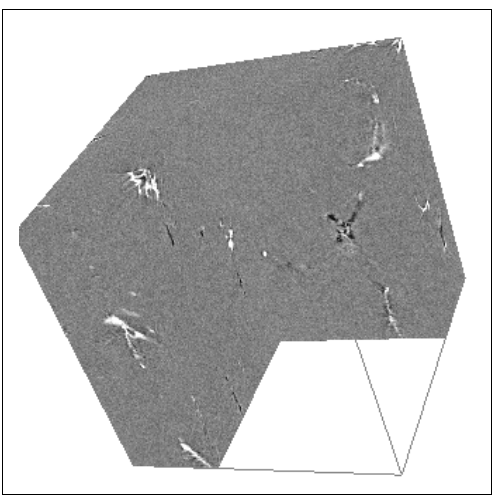

Notes: white – Al_xFe; dark grey – Mg_2Si; black voids – in grey aluminium matrix.

In the following paragraphs, the three-dimensional images analysed in the study are presented. The reason why the X-ray microtomography method was chosen is explained. Then the conditions of observation are presented.

Figure 1 shows the image of the 5xxx aluminium alloys. This image was obtained from ‘line 19’ at the European Synchrotron Radiation Facility (ESRF Grenoble, France). The technique used is X-ray microtomography. In the previous studies, a selective dissolution method was used to observe the internal microstructure of the aluminium

alloy with a SEM. The particles observed with the SEM showed a complex shape, which it is impossible to define with a simple two-dimensional acquisition method. It appeared that a three-dimensional study was required, to be able to do measurements on the 3D complex shape of the particles. X-ray microtomography appeared to be the only method which gives three-dimensional quantitative information on the studied material in a nondestructive way. It provides a possibility to make different measurements on a single sample by changing the resolution of images or by observing each step of the material's evolution during mechanical tests.

The conditions of the acquisition and processing of 3D images were as follows:

- operating conditions: 20 KeV, 0.8 sec, 1500 views, 25 mm
- resolution: 0.7 to 0.28 μm
- grids and connectivity: cubic grid, 26-connectivity.

3 Three-dimensional segmentation

In the first step, it is necessary to threshold images to make measurements on each population of particles. Different methods were tested, but none was really efficient to separate the two types of particles. Finally, a method was designed that was able to perform a multiclass thresholding.

The method used for the segmentation is divided into three main parts. In the first step, the image is filtered. Then a multiclass thresholding is applied. The last part is a combination of the results obtained in the second step, as illustrated in Figure 2.

Figure 2 Schematic description of the segmentation

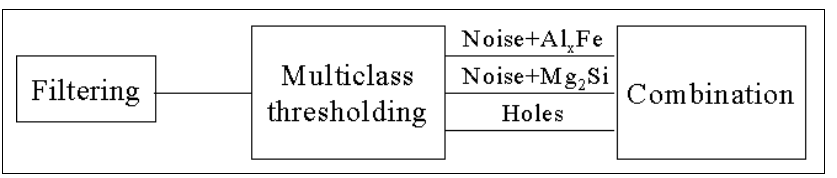

3.1 Filtering

Small local grey value fluctuations of the raw image are not significant. The desired image enhancement should be made without a loss in the sharpness of the image. A 3D Gaussian filter is applied to smooth the image (Klette and Zamperoni, 1996). At present this kind of filter is the best compromise between spatial and frequency locations (Cocquerez and Philipp, 1995).

3.2 Multiclass thresholding

Each type of particle is thresholded separately from the others with a high and a low threshold. In this step, the resulting population is not well segmented, and it contains artefacts due to the image acquisition. This artefact results from the phase contrast in X-ray microtomography images. It is fundamental to separate all types of particles with microtomography. Indeed, while voids and iron-bearing particles are easy to detect,

Mg_2Si particles have almost the same grey level as the aluminium matrix, so that it is not possible to extract them correctly from absorption contrast images. To increase the grey level difference between Mg_2Si and the matrix, a phase contrast is used and the image is saturated in black and white levels. It generates a halo artefact in the surrounding area of the particles. For example, the halo appearing around iron particles has the same grey level as Mg_2Si, while the one around voids and Mg_2Si shows the same grey level as Al_xFe. Thus a combination of all available information has to be used to remove the artefacts from the thresholded images.

3.3 Combining images

A combination of various images is made to extract the halo artefact on a given population, for instance 'Al_xFe'. Firstly, since the phase contrast appears around the other type, 'Mg_2Si+Voids' in our example, a simple dilatation of 'Mg_2Si+Voids' eliminates the halo. A dilatation of 'Mg_2Si+Voids' is performed with a 3D structuring element. An octahedron is chosen with a diameter ranging from five to ten voxels. The size of the applied dilatation depends on the image (on the phase contrast size). Different tests were made to find the best choice. Secondly, the inverse of the dilated 'Mg_2Si+Voids' is taken. Finally, we take the union of the two dilated and inverted images 'Al_xFe' and 'Mg_2Si+Voids'.

3.4 Results

The obtained result is a thin segmentation of each type of particle, as illustrated in Figures 3 and 4. Figure 3 presents the result of the segmentation of Figure 1. Figure 4 shows each type of particle separately.

Figure 3 Example of thresholded image (displayed with the Aphelion© software)

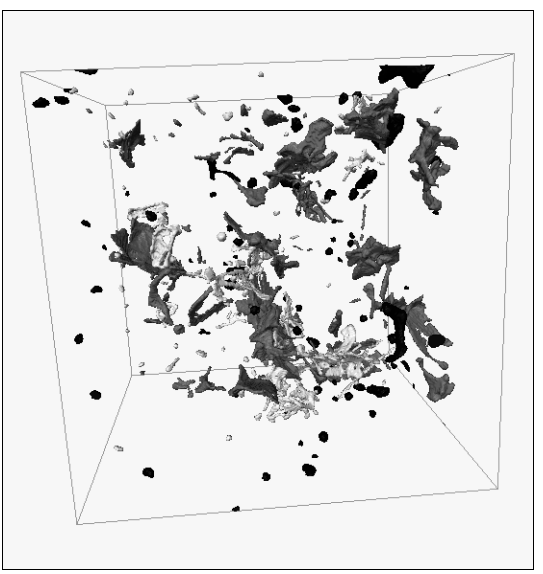

Notes: black – voids; dark grey – Al_xFe; grey – Mg_2Si.

Figure 4 Segmented particles: (a) Mg_2Si; (b) Al_xFe; (c) voids

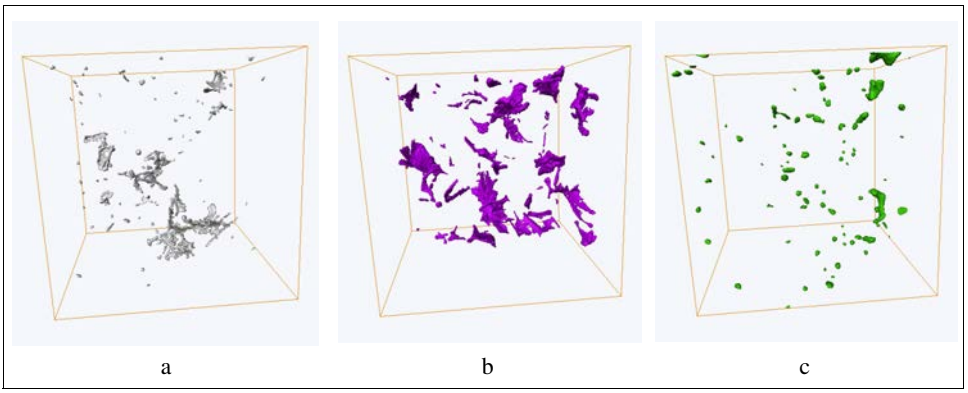

a b c

4 Three-dimensional characterisation

The aim of the three-dimensional characterisation is to characterise the shape of the particles to enable understanding of their ability to break up during the hot rolling process.

Some of the three-dimensional models of particles, such as elliptical, spherical, or characterisation by Fourier analysis, are presented in the literature (Holboth and Vedel Jensen, 2002; Holboth *et al.*, 2002; Delarue and Jeulin, 2003). These descriptions are available for simple 3D shapes or star-shaped particles. In the studied aluminium alloy, the particles show a complex shape. It was not possible to characterise them with simple 3D models. Hence, another approach different from the 'classical' 3D shape characterisation was needed. This section overviews a method to characterise the 3D shape by using morphological measurements.

Since the particles were segmented, it was possible to perform three-dimensional measurements on each of them, and to classify them into families with different shapes. In this section, a set of morphological parameters is provided for characterising 3D complex shapes. Two types of measurements can be performed to obtain distribution measures and parameter values (Aubert and Jeulin, 2000). Distribution measures are distribution graphs, which describe for each particle its properties with respect to a morphological operation. Parameter measurements are made on each particle, describing its shape in order to predict its ability to be broken during the rolling process.

4.1 Classical morphological measurements

4.1.1 Volume

The volume of each particle of a given population Al_xFe, Mg_2Si, or void is estimated by the number of voxels it contains.

4.1.2 Surface area

The surface area is estimated by the method of Crofton (1868). The surface area is proportional to the average of the projected area on several planes of the space, as given by Equation (1). A very good approximation of the surface area (with an error of 4%) is obtained from ten projections:

$$S = 4\langle A_p \rangle. \tag{1}$$

4.1.3 Index of sphericity

This index, given by Equation (2), compares the studied shape to a sphere. It is equal to 1 for a sphere and its value is very sensitive to the object boundary noise:

$$\mathrm{I}_{S_i} = 36\pi \frac{Volume^2_{object_i}}{Surface^3_{object_i}}. \tag{2}$$

A similar type of index, the index of compacity, is obtained by changing the proportionality constant, since it compares the studied shape to a cube.

4.1.4 Geodesic measurements

Geodesic measurements are defined in terms of the geodesic distance (Coster and Chermant, 1989; Lantuejoul and Maisonneuve, 1984). For a given set X, the geodesic distance between two points x_1 and x_2 belonging to X satisfies the following:

- The path connecting x_1 to x_2 is completely included in X.
- The path connecting x_1 to x_2 is the shortest path.

From the geodesic distance, one can define the propagation function of a given point x_1 of X. Its value is given by the maximal length of the geodesic paths (see Equation 3):

$$\forall x_1 \in X, P_x(x_1) = \max\{d_g(x_1, x_2) \mid x_2 \in X\}. \tag{3}$$

4.1.5 Geodesic centre and geodesic radius

The geodesic centre of X is defined as the regional minimum of its propagation function. The presence of noise on the object boundary does not affect the position of the geodesic centre. The value of the propagation function on the geodesic centre is the geodesic radius (see Equation 4):

$$R_g = \underset{x_i \in X}{Inf}\left[\underset{x_j \in X}{Sup}(d_g(x_i, x_j)) \right]. \tag{4}$$

4.1.6 Geodesic length

The geodesic length of X is defined as the length of the longest geodesic path included in X. It is the maximal value of the geodesic propagation function on X, as given by Equation (5):

$$L_g = \underset{x_i, x_j \in X}{Sup} [d_g(x_i, x_j)]. \quad (5)$$

It is not sensitive to the presence of noise on the object boundary. It gives an idea of the studied object complexity, if it is compared to its Feret diameter, and of the geodesic radius.

4.1.7 Orientation parameters

Orientation parameters are calculated for each particle of the aluminium alloy. The orientation of the particle controls, in relation to its shape, its breaking during hot rolling. If the particle is orthogonal to the axis of the applied stress, and if it presents a thin shape, it is clear that it will be easily broken in the first stages of the rolling process. If it presents a thin shape parallel to the rolling axis, then the aluminium matrix will easily slide on the particle without causing any breaking. To estimate the orientation parameters, first the inertia matrix of the particle centred on its mass centre is calculated. Then, the principal axes of inertia are determined. The main axis defines the direction that contains the maximal information about the orientation of particles with respect to the orientation of the rolling process. It also gives some information about the shape, if two or more axes carry the same inertia.

4.1.8 Inertia

To calculate the moments of inertia of a given 3D object belonging to an image, the usual physical laws are used. For those calculations the mass distribution is supposed to be uniform. The elementary volume is equivalent to a voxel. The centre of gravity or centre of mass is defined by Equation (6):

$$\overrightarrow{OG} = \frac{\sum_i m_i \cdot \overrightarrow{OA_i}}{M} \quad (6)$$

where:

'O' = the image origin
'G' = the centre of mass
'M' = the mass of the object
m_i = the elementary mass equal to 1 in the case of an image.

The matrix of inertia is given by the general formula in Equation (7):

$$[J_0] = \begin{pmatrix} \sum m_i(y_i^2 + z_i^2) & -\sum m_i(y_i \cdot x_i) & -\sum m_i(z_i \cdot x_i) \\ -\sum m_i(y_i \cdot x_i) & \sum m_i(x_i^2 + z_i^2) & -\sum m_i(y_i \cdot z_i) \\ -\sum m_i(z_i \cdot x_i) & -\sum m_i(y_i \cdot z_i) & \sum m_i(x_i^2 + y_i^2) \end{pmatrix}. \quad (7)$$

4.1.9 Principal orientation

From the inertia matrix, it is possible to obtain the three principal moments of inertia of particles, given by the eigenvalues of the matrix (see Equation 7). The orientation of the axis of inertia is deduced from the eigenvectors P of the matrix (see Equation 8). The principal axis, with the highest moment, is taken as a reference to calculate the orientation of the particles:

$$P = \underbrace{\begin{pmatrix} u_{11} & u_{21} & u_{31} \\ u_{12} & u_{22} & u_{32} \\ u_{13} & u_{23} & u_{33} \end{pmatrix}}_{\overrightarrow{u_1}\,\overrightarrow{u_2}\,\overrightarrow{u_3}}. \tag{8}$$

The angles between the axis of inertia and the axis of the image (see Figure 5) are calculated. Figure 6 presents the projected direction of the principal axis of each iron-containing particle of a 2% deformation aluminium alloy in the unit sphere; a uniform distribution of the orientation of particles is observed after a 2% deformation.

Figure 5 Definition in space of the orientation of the principal axis, with Euler angles

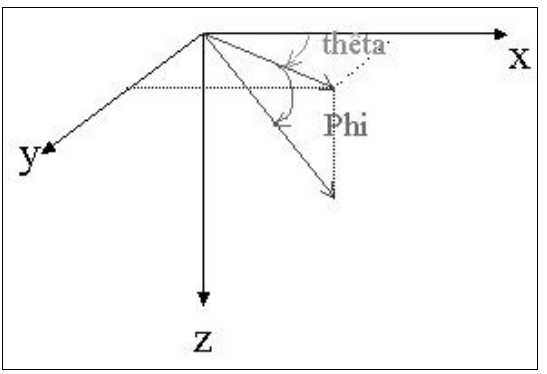

Figure 6 Stereographic projection of the principal axis for 4000 particles in an alloy at 2% deformation (see online version for colours)

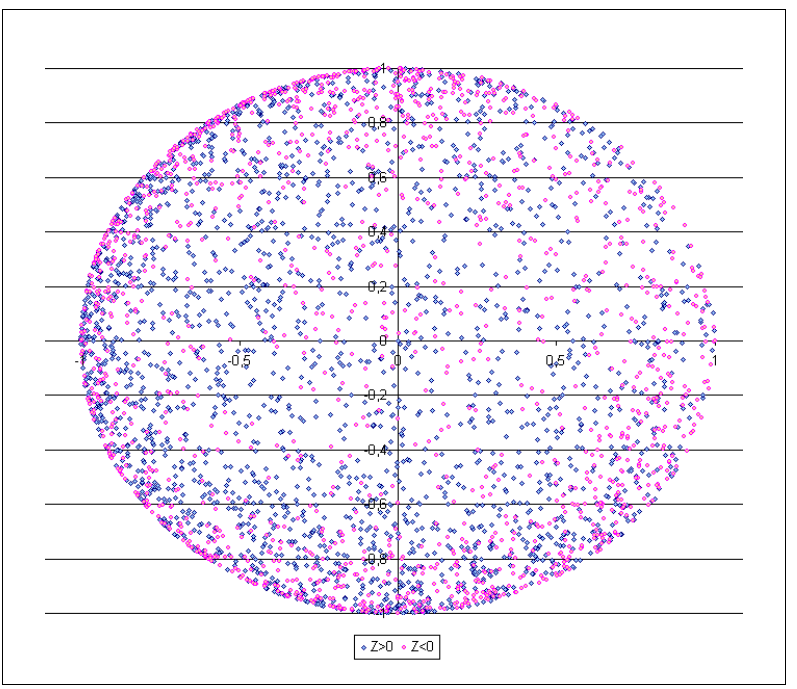

4.1.10 Opening of particles

The *local granulometry* of a particle by morphological openings is the distribution of the object size with respect to the structuring element used for the opening (octahedron with a diameter ranging between 1 and 10 pixels). It gives an idea of the shape of the studied object by considering the evolution of the distribution depending on the step of the opening λ. The inflection points of the granulometry distribution give the mean thickness of the studied particles.

The *local connected component number* is the number of distinct parts of an object at each step of the granulometry. It depends on the neighbourhood used for the image computation. A '26 connected graph' is used in this study because of the presence of thin connections. The evolution of the number of connected components of the local granulometry by opening transformations gives an indication of the complexity of the shape and the aptitude for the particle to be broken into several parts.

5 Results

Some results of 3D morphological measurements are given to illustrate two typical particles extracted from the population of intermetallic particles (about 4500 particles of iron-containing particles) in a 10% deformation aluminium alloy (Figure 7a–b). The presented particles show a different shape. Particle (a) is compact, particle (b) is not, being made of a structure of thin branches:

Particle (a) The granulometry shows that the mean thickness of (a) is between seven and eight voxels. The connected component number shows that the particle is never broken at any step of the opening until it disappears suddenly, because the size of the erosion applied during the opening becomes larger than the particle size. This particle does not seem to be easily breakable under a load. Other parameters seem to confirm this point. R_g is large (a value of 10), indicating that the particle is able to contain a ball with a radius equal to 10, its core having a large size. L_g has a value similar to R_g, the particle not being very elongated and presenting no point of weakness.

Particle (b) The granulometry shows that the mean thickness of particle (b) is nearly two to three voxels. The connected component number shows that the particle is broken up into different parts (13 at the maximum) at each step of the opening. This particle seems to be easily broken under a load. Other parameters strengthen this observation. R_g is very low (one voxel), showing that the particle has a bottle-shaped neck. L_g is really larger than R_g and the mean thickness is deduced from the granulometry. The particle is not compact and seems to be flat, the surface area being close to the volume. The branches are made of thin planes.

Figure 7 Single iron-containing particles with their local granulometry by opening and connected component number for each step of the opening by an octahedron-structuring element (see online version for colours)

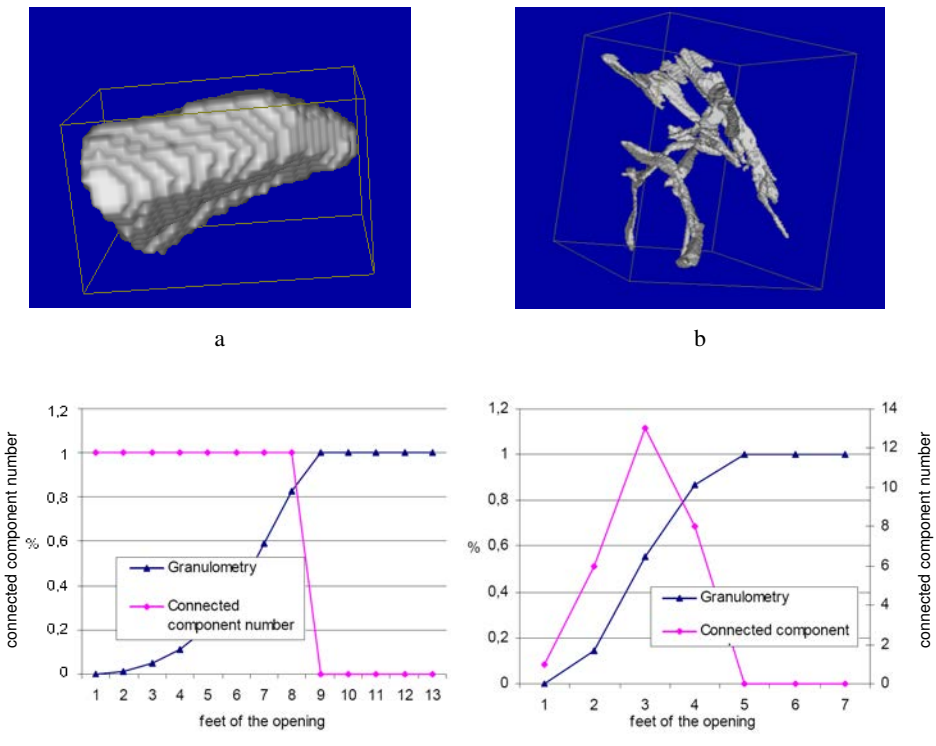

	I_c	I_s	V	S	L_g	R_g	D_f
a	0.27	0.48	4302	1631.5	59	10	45
b	0.0046	0.0086	20 530	17 658	255	1	216.2

Note: The 3D morphological measurements on each particle (a and b) are given in the table.

5.1 Example of application

The results are given for two stages of deformation of the aluminium (10% and 82%). The goal of the study was to use the statistical distribution of parameters to expose the microstructural differences (changes of shape of the particles) caused by mechanical stress applied during the hot rolling process.

Our observation focused first on the study of the stereographic projection of the orientation of the particles (Figure 8). For the early stage of deformation (10%, Figure 8a), the particles were uniformly oriented in space. For a high stage of deformation (82%, Figure 8b), the results of the stereographic projection of the orientation of particles indicated that the particles were given a privileged orientation along the rolling axis. The particles were arranged like parallel sheets towards the (x, y) plane, which corresponded to the rolling plane.

Figure 8 Stereographic projection of principal axes of each particle for a deformed sample of aluminium alloy at two different stages of deformation: (a) 10% of deformation; (b) 82% of deformation (see online version for colours)

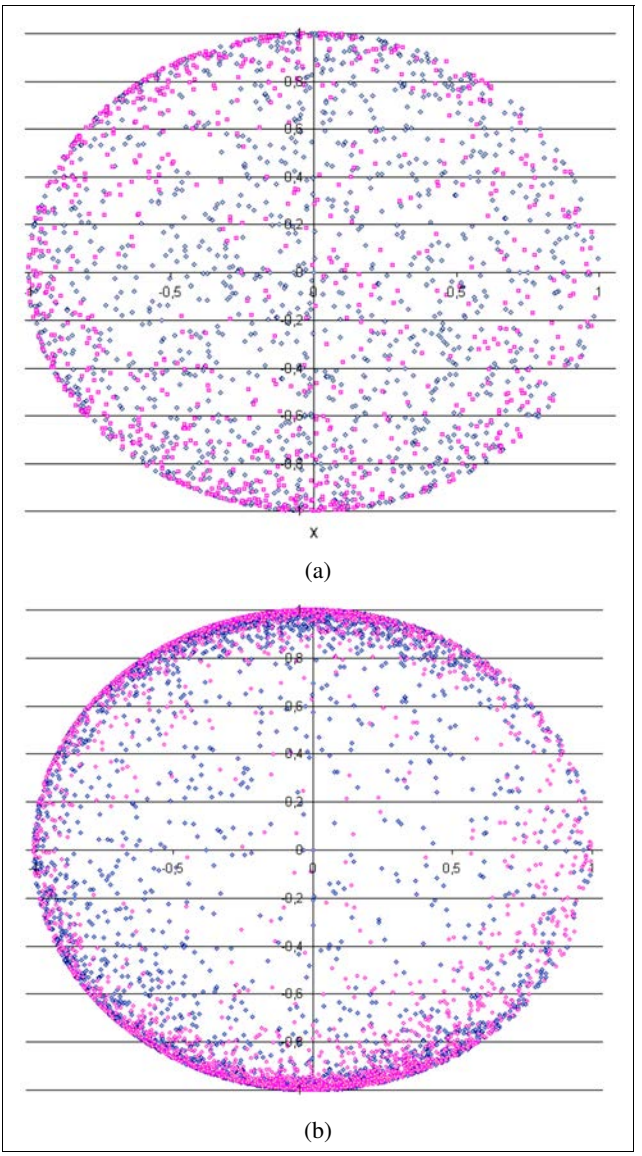

We looked at the other results to understand the internal mechanism that occurs during the rolling process. The results of the measurements are presented in Figure 8 as the distribution in volume (each particle was counted proportionally to its volume) of the volume, the surface area and the sphericity index for the two stages of deformation (10% and 82%). The χ^2 tests on each histogram of the two samples showed that there was a significant evolution of the distribution of the surface area and of the volume of particles, whereas there was no significant change for the index of sphericity (the particle did not become spherical). From the spatial distribution of the volume, we observed that the

particles were broken by the applied stress, as was indicated by the larger population of particles with a volume lower than 3000 μm^3 in the alloy deformed at 82%. The same observation was made on the surface area distribution, where the population of particles with a small surface area increased during deformation.

Figure 9 Spatial distribution of particles in a deformed sample of aluminium alloy at two different stages of deformation (10% and 82%); (a) volume, (b) surface area, (c) sphericity index (see online version for colours)

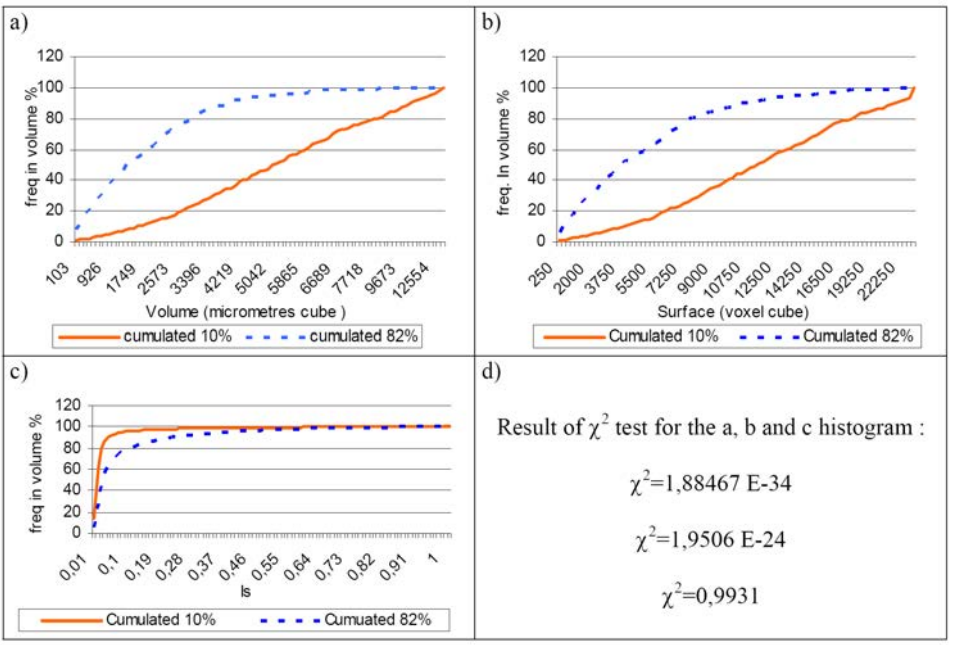

These results confirm the assumption that the particles took a position that reduced the effect of the mechanical stress induced by hot rolling. Large particles were broken but their shape did not become spherical or cubic.

Additional studies shall be made to compare particles at other stages of deformation of the plate. A statistical study will be made in order to classify particles into families that present the same morphological characteristics regarding their mechanical behaviour. Their evolution will be followed during the rolling process.

6 Conclusion

In this paper, we have presented a set of morphological parameters adapted to the characterisation of 3D complex shapes.

An analysis of the evolution of the population of intermetallic particles at different stages of the rolling process was performed.

Statistical analysis by principal component analysis should be applied to highlight the trend of intermetallic particle shapes, and to study the evolution of types of shapes during the industrial process (Parra-Denis *et al.*, 2006).

Acknowledgements

This project was supported by Région Rhône Alpes. The authors are grateful to the members of the involved consortium, composed of Alcan CRV (Annabelle Bigot, Stéphane Savelli), ESRF id 19 (Jose Baruchel, Petra Pernot), INSA Lyon (Eric Maire) and École des Mines de Saint-Étienne (Helmut Klocker, Matthieu Feuerstein, Nicolas Moulin).

References

Aubert, A. and Jeulin, D. (2000) 'Classification morphologique de surfaces rugueuses', *Revue de Métallurgie-CIT/Science et Génie des matériaux*, pp.247–262.

Baldacci, A. (2003) 'Rupture des particules intermétalliques durant le laminage à chaud d'un alliage d'aluminium 5182', PhD thesis, Ecole des Mines de Saint-Etienne.

Buffiere, J., Maire, E., Cloetens, P., Lormand, G. and Fougeres, R. (1999) 'Characterization of internal damage in a MMCp using X-ray synchrotron phase contrast microtomography', *Acta Materialia*, Vol. 47, pp.1613–1625.

Cocquerez, J.P. and Philipp, S. (1995) *Analyse d'images : filtrage et segmentation*, Chap. 4, Masson.

Coster, M. and Chermant, J.L. (1989) 'Squelettisation et transformations de voisinage', Chap. 6 in *Précis d'Analyse d'Images*, CNRS Press, pp.195–209.

Crofton, M.W. (1868) 'On the theory of local probability, applied to straight lines drawn at random in a plane; the methods used being also extended to the proof of certain new theorems in the integral calculus', *Phi. Trans. of Royal Soc. London*, No. 158, pp.181–199.

Delarue, A. and Jeulin, D. (2003) '3D morphological analysis of composite materials with aggregates of spherical inclusions', *Image Anal Stereol*, Vol. 22, pp.153–161.

Feuerstein, M. (2006) 'Influence de la microstructure sur les propriétés mécaniques de tôles d'aluminium AA5182', PhD thesis, Ecole des Mines de Saint-Etienne.

Holboth, A., Pedersen, J. and Vedel Jensen, E. (2002) 'A deformable template model, with special reference to elliptical models', *Journal of Mathematical Imaging Vision*, Vol. 17, pp.131–137.

Holboth, A. and Vedel Jensen, E. (2002) 'A stereological analysis of shape', *Image Anal Stereol*, Supplement 1, pp.S23–S29.

Klette, R. and Zamperoni, P. (1996) *Handbook of Image Processing Operators*, Chap. 6, Wiley.

Lantuejoul, C. and Maisonneuve, F. (1984) 'Geodesic methods in quantitative image analysis', *Pattern Recognition*, Vol. 17, p.177.

Parra-Denis, E., Barat, C., Ducottet, C. and Jeulin, D. (2005a) '3D morphological analysis of particles in aluminium alloys by X-ray microtomography', *EUROMAT 2006*, Prague, Czech Republic.

Parra-Denis, E., Barat, C., Ducottet, C. and Jeulin, D. (2006) 'Caractérisation morphologique de particules intermétalliques dans les alliages d'aluminium par analyse statistique', *Matériaux 2006*, Dijon, France.

Parra-Denis, E., Ducottet, C. and Jeulin, D. (2005b) '3D morphological analysis of non metallic inclusions', *9th European Congress on Stereology and Image Analysis and 7th STERMAT International Conference on Stereology and Image Analysis in Materials Science*, Polish Society of Stereology, pp.111–122.

Soille, P. (1999) 'Opening and closing', Chap. 4 in *Morphological Image Analysis Principles and Applications*, Springer, pp.111–113.